Microstructure evolution and creep behaviour of a new intermetallic alloy

G. Angella, E. Festari, V. Lupinc, M. Maldini, E. Signorelli, O. Zanon
Istituto IENI – Consiglio Nazionale delle Ricerche - Unità organizzativa di Milano - Milano - Italy

ABSTRACT

The preliminary results of microstructural characterization and creep behaviour of an innovative TiAl 8% atomic Nb alloy are exposed in this paper. Two different batches of this material, with same nominal chemical composition, but produced through different solidification processes and heat treatments, have been studied. The production processes generated different $\gamma + \alpha_2$ microstructures in the two batches, both analyzed through X ray diffractometry (XRD) and transmission electron microscopy (TEM). Constant load creep tests have been performed on both batches at the same temperatures (700°C and 850°C) and loads in order to compare the creep behaviours. XRD and TEM analyses have been carried out after creep tests in order to determine microstructural evolution of the materials and to establish correlation with creep behaviours.

RIASSUNTO

Nella seguente memoria sono presentati i risultati preliminari relativi alla caratterizzazione microstrutturale congiunta al comportamento a creep di una lega innovativa TiAl contenente 8% atomico di Nb. Sono stati studiati due diversi lotti del materiale, aventi la medesima composizione chimica nominale, ma caratterizzati da processi di produzione e storie termiche distinte, che hanno dato luogo a microstrutture $\gamma + \alpha_2$ diverse nei due lotti. Entrambe le microstrutture sono state analizzate mediante diffrattometria ai raggi X (XRD) e microscopia elettronica in trasmissione (TEM). I due lotti sono stati sottoposti a prove di creep a carico costante alle medesime temperature, 700°C e 850°C, ed ai medesimi carichi in modo da confrontarne il comportamento a creep. I due lotti hanno avuto comportamenti a creep distinti e le osservazioni XRD e TEM sono state compiute anche sui materiali sottoposti a creep in modo da definire l'evoluzione microstrutturale e correlare tale evoluzione con i comportamenti a creep.

INTRODUCTION

The intermetallic TiAl alloys with $\gamma + \alpha_2$ structure are subject of extensive research, because these materials could be used in production of aero-engines and terrestrial gas turbine blades. High Al percentage, which causes the very good oxidation strength of these materials, their low density (half of that of superalloys) and high Young modulus make them very attractive for applications in rotor components operating at high temperatures [1, 2]. Besides these advantages, the principal applicative restrictions of TiAl alloys are their low ductility at room temperature [3] and low reproducibility of microstructure and mechanical properties, caused by the presence of raw solidification

microstructures and significative micro-segregations.

One way to obtain fine microstructures from fusion products without involving temperature deformation processes consists in exploiting the massive transformation through intermediate cooling rates [4, 5], which begins during the cooling from phase α field and becomes a metastable phase with an high defects density, called massive gamma, i.e. γ_M. This massive transformation is particularly significative in TiAl alloys containing Nb and Ta: this is the main reason why Nb was used too alloy TiAl in the present investigation. The γ_M phase is chemically indistinguishable from the parent phase α, and has a CFC not ordered structure that is chemically and crystallographically different from the intermetallic γ phase. There are two benefits on the fusion products: first, with the massive transformation the grain size remains small; secondly, the metastable γ_M phase has a high density of defects (dislocations, micro-twinning and antiphase borders), and if the material with this structure is heated up to the $\gamma+\alpha$ field, these defects become nucleation sites of α phase on the {111} planes of the γ_M phase. The high density of nucleation sites produces a diffuse and homogeneous lamellar structure, called Deconvoluted Cross Lamellar Structure (DCLS) that gives homogeneous and isotropic mechanical properties to the material, with a higher ductility at room temperature.

This paper presents the preliminary results aimed at the realization of last generation TiAl alloys with Nb and Ta, developed in the European integrated project IMPRESS, part of the VI Frame Program. This project includes 42 European partners among Research Centres, Universities and companies. One of the first aims of the IMPRESS project is the production of a low pressure 40 cm long gas turbine blade of intermetallic TiAl base alloy. The work of IENI-CNR Institute in Milan in the IMPRESS project was the characterization of creep behaviour properties of selected alloys. In this paper the preliminary creep behaviour results of two different batches of a last generation TiAl alloy are reported, the outcome of microstructure analysis and a first rationalization of the relationship between microstructure and creep behaviour.

MATERIALS AND EXPERIMENTAL PROCEDURES

The TiAl-8Nb alloy (nominal composition 46Ti-46Al-8Nb in atomic %) is one of the intermetallic alloys selected in the IMPRESS project for production of gas turbine blades. The alloy presents a $\gamma + \alpha_2$ structure, where γ (TiAl) is the intermetallic tetragonal ordered ($L1_0$) phase, and α_2 (Ti_3Al) is the intermetallic hexagonal dense ordered ($D0_{12}$) phase. The two batches of TiAl-8Nb alloy, supplied by IRC in Birmingham (UK) and ACCESS in Aachen (D) in the form of 13 mm diameter cylindrical bars, have been obtained through two different production routes:
1) batch E, obtained through centrifugal casting solidification;
2) batch BN, bars obtained with electro erosion from ingot produced through conventional plasma furnace.

After solidification, the two batches have been exposed to similar heat treatments:
- a solubilisation heat treatment up to 1360°C for 1 hour, followed by quenching in oil;
- a Hot Isostatic Pressing (HIP) treatment at 1310°C for 4 h with 150 MPa, followed by cooling, for batch E;
- a HIP treatment at 1280°C for 4 h with 150 MPa, followed by a 4 h heat treatment up to 1280°C and successive cooling, for batch BN.

The chemical compositions of the alloy in the two batches, obtained through Energy Dispersion Spectroscopy (EDS), are showed in the following table I. The measured percentages are considerably different from the nominal ones, as batch E has an Nb percentage identical to the nominal one, whereas batch BN has a higher one. Besides, the Ti/Al ratio is bigger in batch E than in batch BN.

Constant load creep tests have been carried on 28 mm gauge length and 5.6

Table I. Chemical Composition in atomic % of batch E and BN.

Batch	Ti	Al	Nb
E	46.9 ± 0.3	44.8 ± 0.4	8.3 ± 0.2
BN	46.1 ± 0.3	44.9 ± 0.4	9.0 ± 0.2

mm gauge diameter cylindrical specimens. Creep strain was continuously monitored using two capacitive transducers, placed outside the furnace and connected to the specimen. At least two hundred strain/time readings were recorded throughout each creep test. Three thermocouples were placed on the gauge surface in order to measure the temperature and its gradient along the specimen axis. Partial loading at room temperature was performed in order to determine the Young modulus of the alloy. Before the effective start of any test, the specimens were left at test temperature for an amount of time between one and three hours long. All strains in this paper are true strains, defined by $\varepsilon = \ln(1 + \Delta l/l_o)$, where l_o and $\Delta l = l - l_o$ are the initial length and the elongation of the specimen gauge length during creep, respectively.

The alloy microstructure was studied using transmission electron microscopy (TEM) and X ray diffractometry (XRD). The latter was performed by means a Siemens D500 diffractometer with Cu target. The volume fraction of γ and α_2 phases was determined through comparison with simulated software-obtained spectra. TEM analysis was performed with a JEM FXII Jeol electronmicroscope, with 200 kV extraction tension. TEM samples have been prepared with electro etching of 3 mm diameter size and 80 μm thickness discs, obtained via mechanical polishing through sandpapers of progressively smaller grain size. The final thin foil perforation was performed electrolytically with a double jet commercial instrument, using a 5% perchloric acid, 60% methanol and 35% butanol electrolyte at -25°C and 20 V applied tension.

EXPERIMENTAL RESULTS

CREEP RESULTS

Creep tests have been performed on both batches at 700°C with 300, 350 and 400 MPa stress, and at 850°C with 100, 150, and 250 MPa stress, in order to produce times to rupture up to 2500 h. The resulting creep behaviour is shown by ε vs. t and $\log\varepsilon$ vs. ε curves reported in Fig. 1-2. As clearly reported by $\log\dot\varepsilon$ vs. ε plots, after a decrease in the primary decelerating regime till a minimal value $\dot\varepsilon_{min}$, the creep strain rate $\dot\varepsilon$ does not show secondary steady regime, but increases in a accelerating regime up to the specimen rupture. Same creep tests performed on both batches show that batch E has lower minimal creep strain rates $\dot\varepsilon_{min}$ and longer time to rupture for the same deformation conditions. Besides, creep curves analysis reveals that the primary regime relevance seems to grow as the stress increases in both batches, and becomes irrelevant after first few percent of strain.

It is interesting to note that during the accelerating regime that comprises almost all the strain, the $\log\dot\varepsilon$ vs. ε curves assume a linear behaviour. Then, the strain rate $\dot\varepsilon$ in the accelerating regime can be related to ε by the following equation:

$$\dot\varepsilon = \dot\varepsilon_o \exp m\varepsilon \qquad (1)$$

where m represents the gradient of the line obtained interpolating $\log\dot\varepsilon$ vs. ε values of accelerating regime, and $\dot\varepsilon_o$ is the extrapolated strain rate at $\varepsilon = 0$; $\dot\varepsilon_o$ and $\dot\varepsilon_{min}$ have similar, but not identical values. It is worth noting that $\log\dot\varepsilon$ vs. ε plots show that the gradient m values are substantially independent from applied stress, and then from creep test time to rupture, even if the latter can vary an order of magnitude. This implies the accelerating regime is caused by a strain connected damage process, instead of a time connected one that could be related to material aging.

As received batch E and BN diffractometry spectra, reported in Fig. 3, show that significant volume fractions of α_2 phase are present in both batches. This fraction is bigger in batch E, 10.0%, than in batch
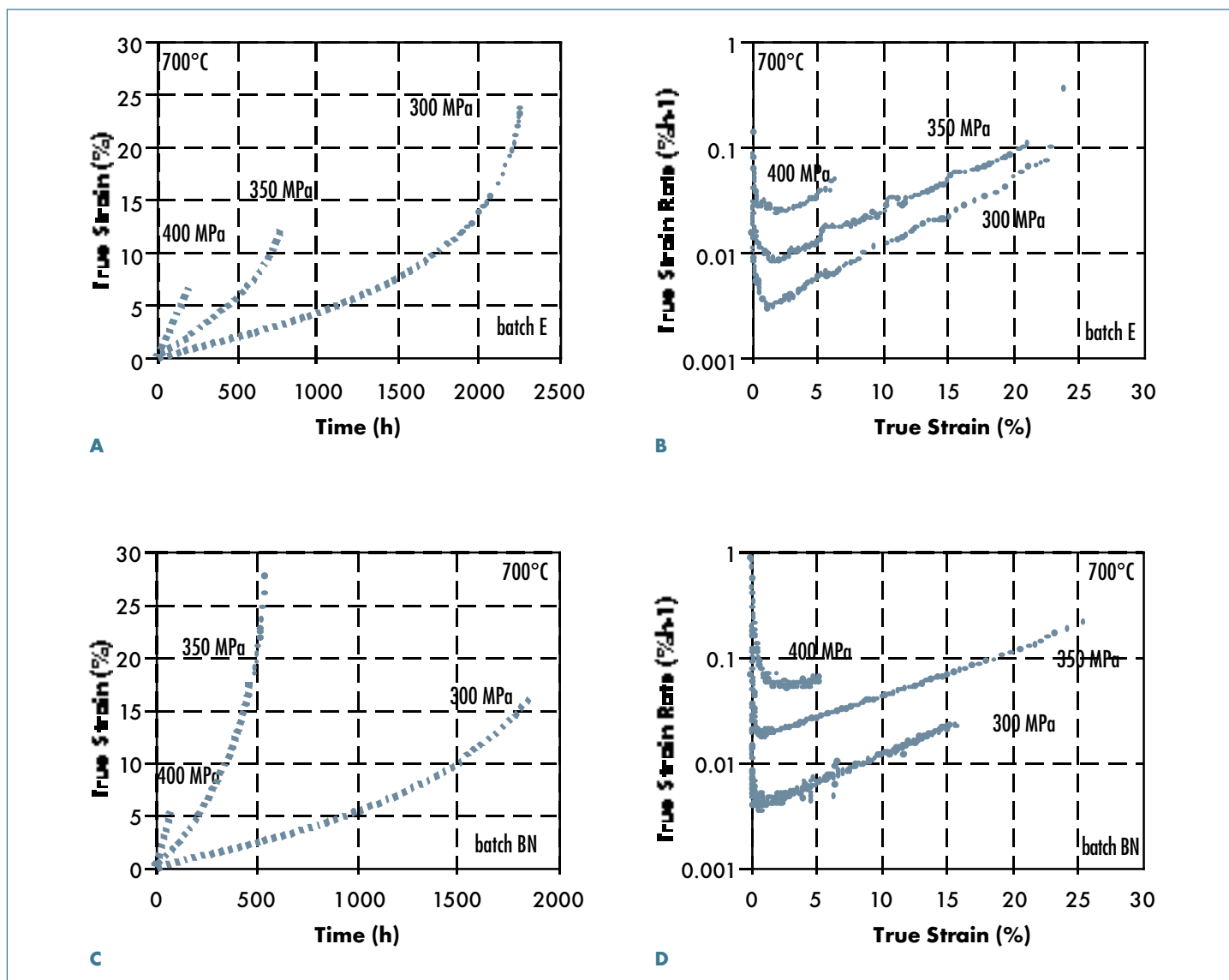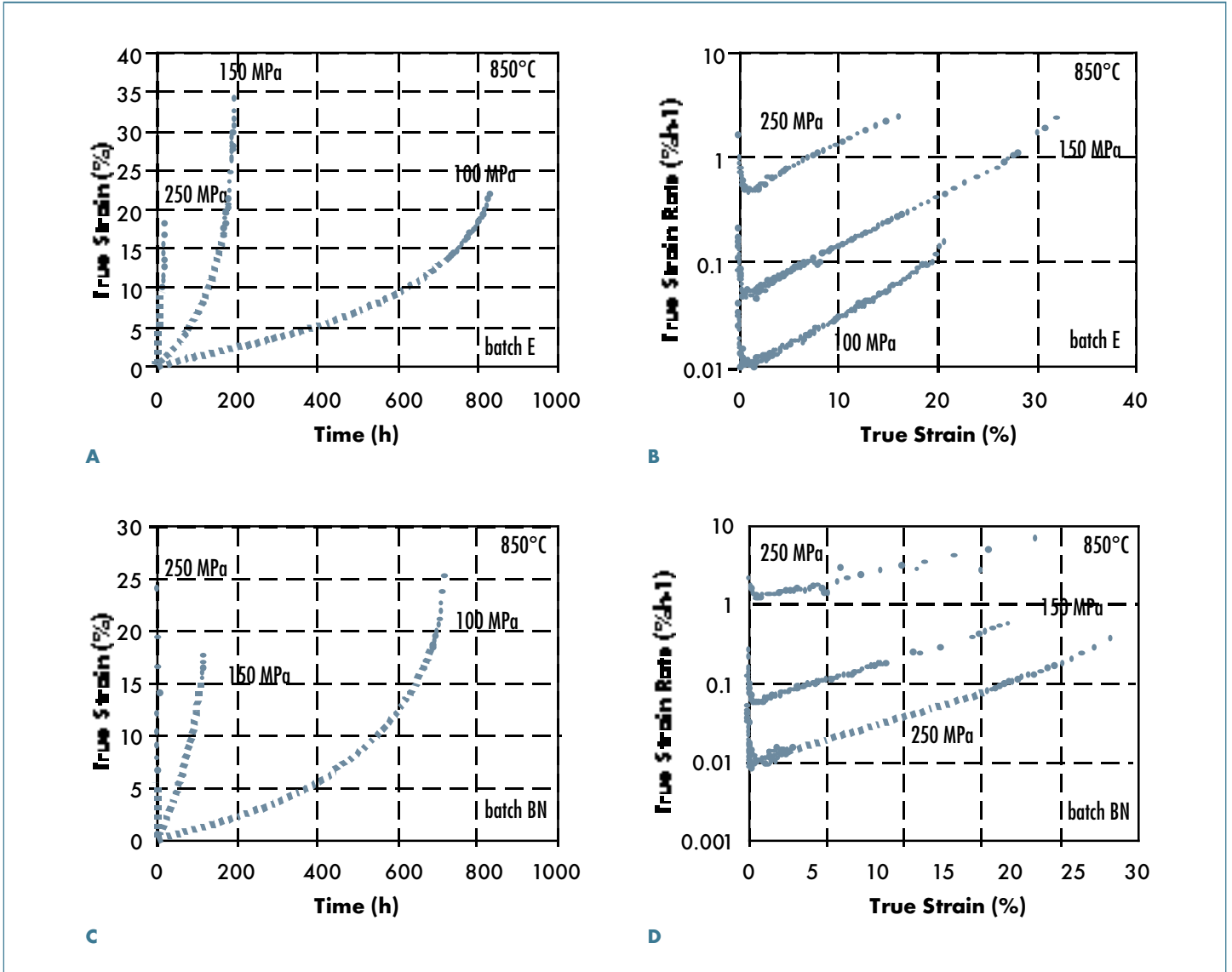

Fig. 1: Batch E: curves (a) ε vs. t, (b) log $\dot\varepsilon$ vs. ε at 700°C; batch BN: curves (c) ε vs. t, (d) log $\dot\varepsilon$ vs. ε at 700°C.

Fig. 2: Batch E: curves (a) ε vs. t, (b) log $\dot{\varepsilon}$ vs. ε at 850°C; batch BN: curves (c) ε vs. t, (d) log $\dot{\varepsilon}$ vs. ε at 850°C.

BN, 6.5%, as expected from the bigger Ti/Al ratio measured in batch E (Tab. I). Diffractometry analysis after 700°C and 850°C creep tests shows that both batches specimens undergo a significant evolution of microstructure from the as received one, both in specimen head (zero stress applied) and in the working section. Diffractometry spectra performed on both batches after 700°C 400 MPa creep test are showed as example in Fig. 4. In the specimen heads, see Fig. 4(a) for batch E and Fig. 4(c) for batch BN, the exposition to test temperatures alone caused in both batches a strong reduction of α_2 phase volume fraction, whose amount is equal to 700°C and 850°C, and independent of creep test
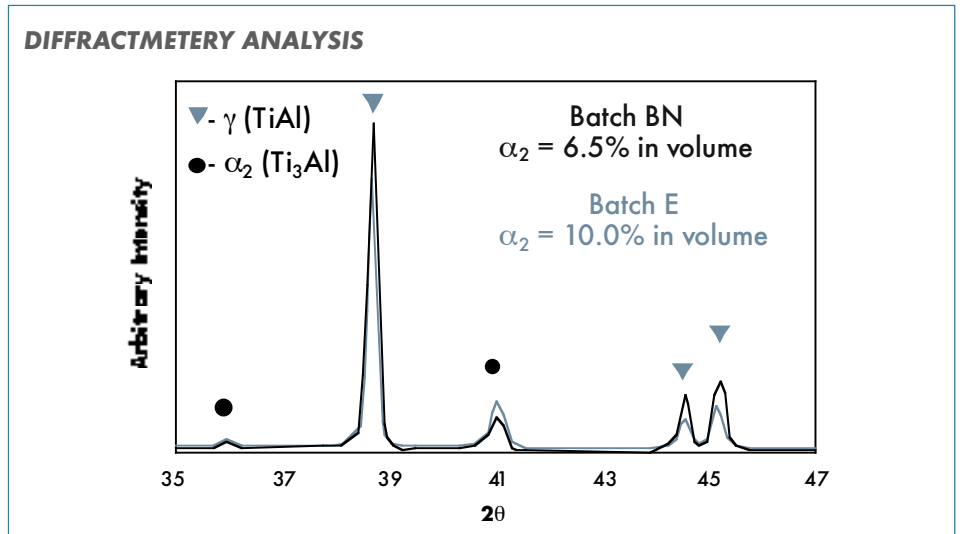
DIFFRACTMETERY ANALYSIS

Fig. 3: As received batch E and BN diffractometry spectra.

duration. Since the exposition time of specimens heads is the creep tests time to rupture, which varies with applied stress of an order of magnitude, from substantially equal values of α_2 phase volume fraction it can be thought that α_2 phase reduction process ends in relative short time.

Fig. 4(b) and Fig. 4(d) spectra, performed on specimens working section, which undergoes creep strain during tests, show lower values of α_2 phase volume fraction. Then, it can be deduced from diffractometry analysis that in both batches the strain caused another evolution of microstructure, which is a further reduction of α_2 phase volume fraction.
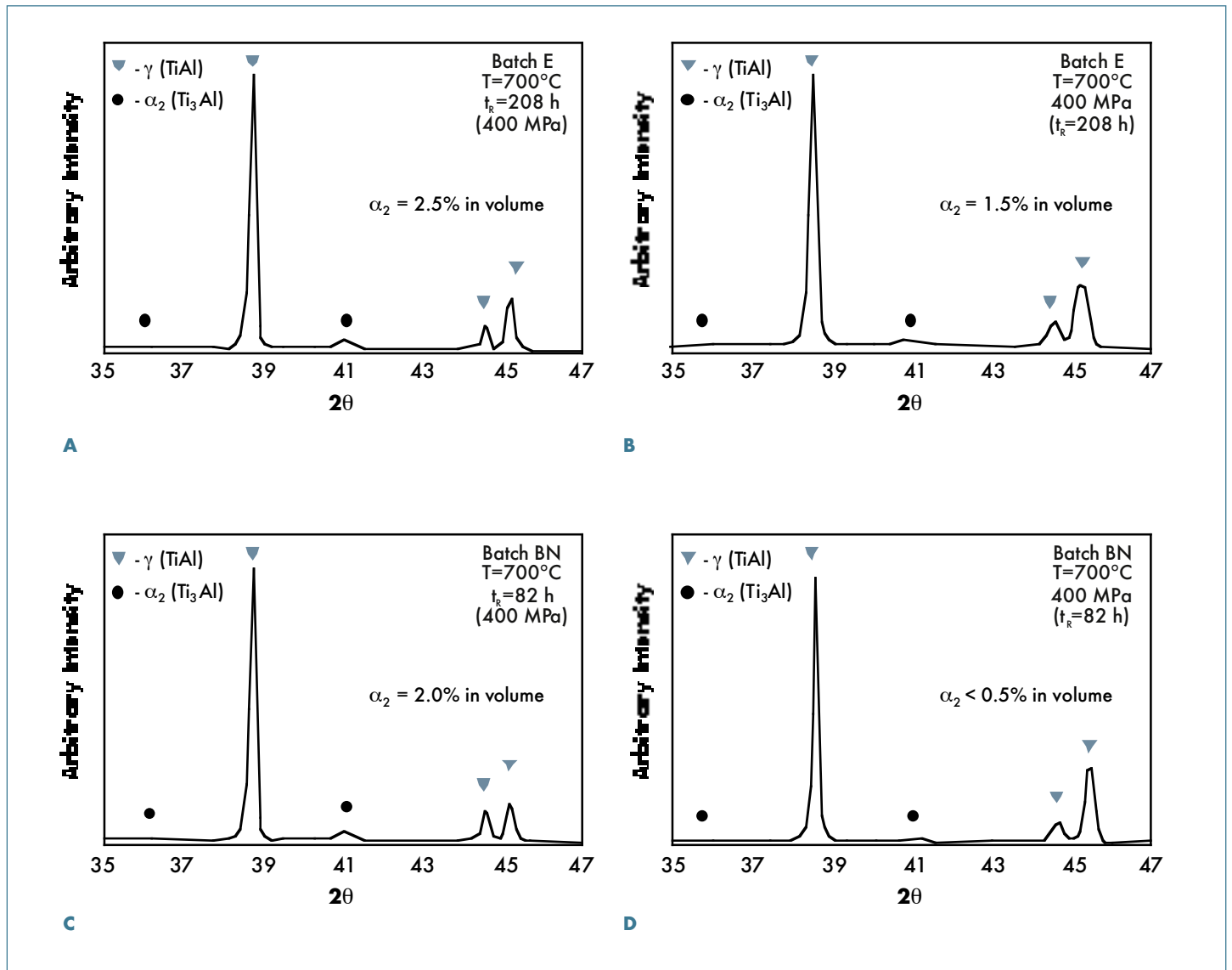

Fig. 4: Batch E: after a 700°C, 208 h long creep test, without stress (a), and with a stress of 400 MPa (b); Batch BN: after a 700°C, 82 h long creep test, without stress (c), and with a stress of 400 MPa (d).

TEM MICROSTRUCTURAL ANALYSIS

Microstructural analysis on samples of the as received alloys was performed through TEM microscopy: some representative micrographs are reported in Fig. 5. In both batches lamellar structures and γ phase grains were observed. While Fig. 5(a) shows that batch E lamellar structures are clearly defined, Fig. 5(c), instead, shows that in batch BN there is a less definite structure, with not parallel, needle-like bigger lamellae. Lamellar structures TEM analysis on each sample was performed through determination of the γ phase crystallographic local axis $B = [0\text{-}11]$: it appeared that both batches lamellar structure is characteristic for TiAl alloys structure [3], with $\gamma + \gamma$ and $\gamma + \alpha_2$ lamellae, related by the crystallographic relationship:

$(111)_\gamma //(0001)_{\alpha2}$ and $(110)_\gamma //(2\ 11\overline{2}0)_{\alpha2}$ (2)
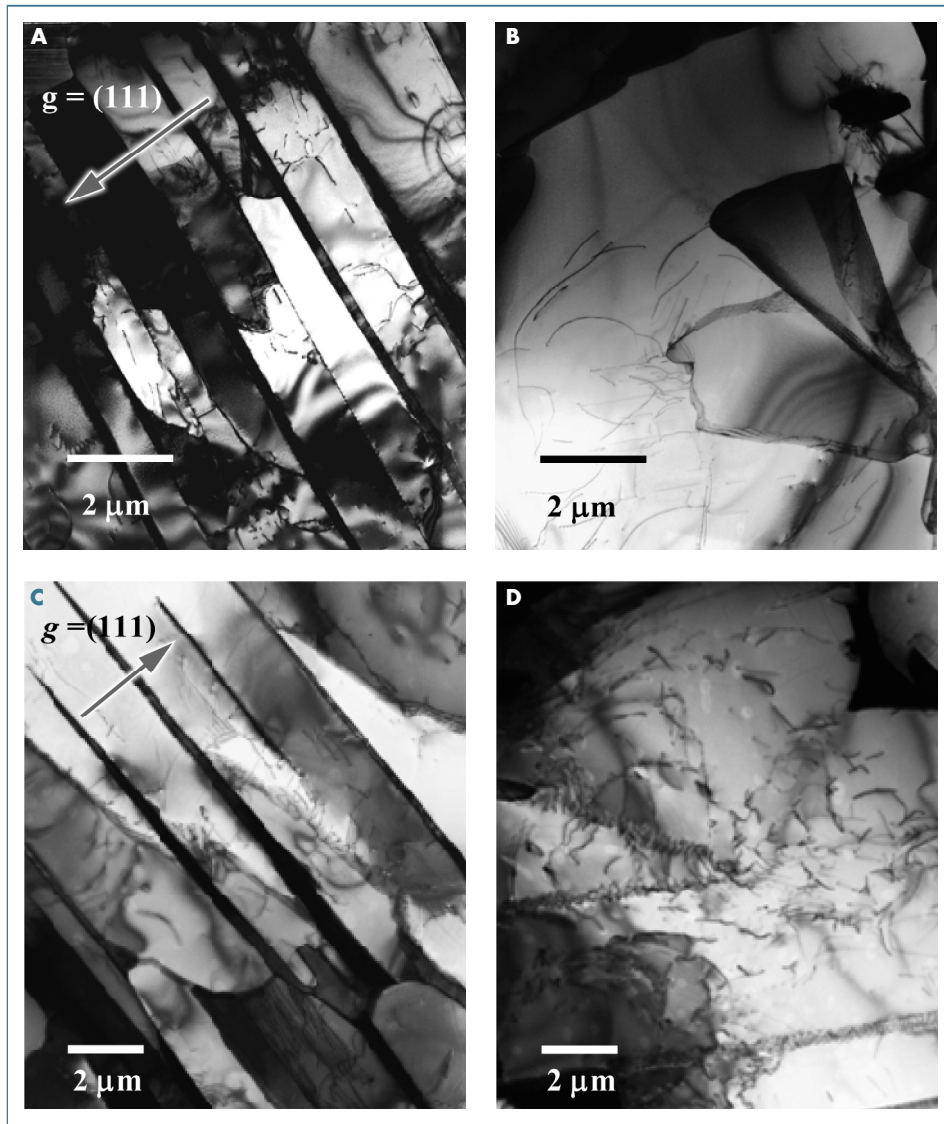
Temperature and stress effects on both

Fig. 5: TiAl-8Nb alloy TEM micrographs: (a) and (b) as received batch E, (c) and (d) as received batch BN; (a) lamellar structure observed on edge (crystallographic local axis B = [0-11]), (b) γ grain; (c) on edge lamellar structure, (d) γ grain dislocative structure.
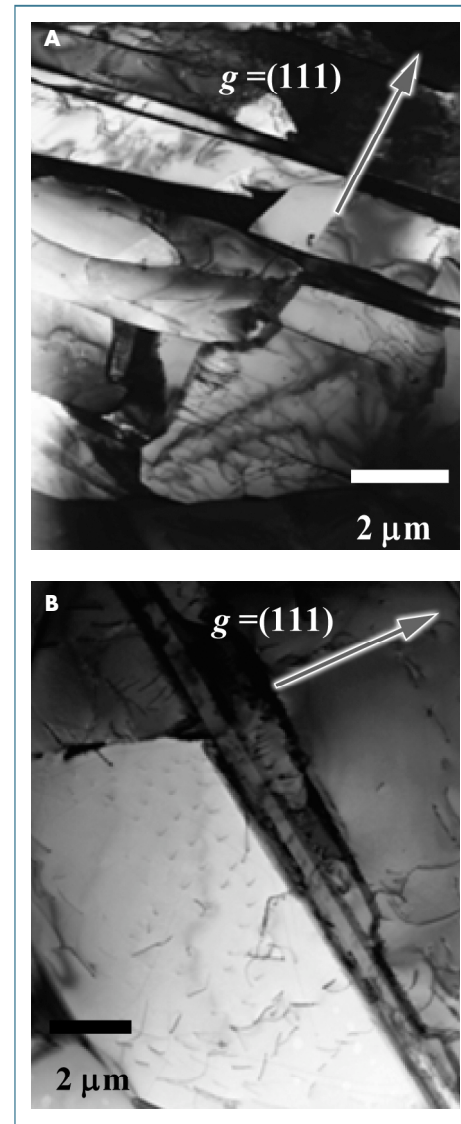
Fig. 6: TiAl-8Nb alloy TEM micrographs after 700°C creep test with zero stress (specimens heads): (a) batch E after 2852 h, local axis B = [0-11]; (b) batch BN after 1850 h, local axis B = [0-11].

batches microstructure were studied through analysing either specimens heads (temperature influence alone) and working section (temperature and creep strain).
Fig. 6 micrographs were performed on samples obtained from specimens heads after a 700°C creep test and show a considerable microstructural evolution from the as received structure in both batches, which was already revealed by diffractometry spectra. Batch E lamellar structure is no longer clearly defined, while batch BN structure presents few lamellar zones, characterized by not clearly defined lamellae, bigger than those seen in the as received samples. It appears clearly from the analysis that the two batches lamellar structures have different characteristic sizes, definitely bigger in batch BN than in batch E.
Fig. 7 micrographs were performed on samples obtained from specimens heads after a 850°C creep test and show that both batches underwent the same microstructural evolution from as received structure. However, in this case the difference between batches resulted particularly relevant: batch E analysis shows that there is still a residual lamellar microstructure, while batch BN appears to have generally a equiaxial γ grain structure, lacking in lamellar zones.

TEM microstructure analysis was performed on specimens working section that underwent creep: micrographs of a batch E specimen after creep at 700°C and 350 MPa, are reported in Fig. 8. Samples obtained after each creep test showed that both batches alloy developed an extremely thin lamellar structure, because of mechanical twinning growth: from Fig. 8(c), diffraction image correspondent to 8(a) and 8(b) morphological images, it is revealed that the diffraction image resulted from superimposition of matrix (—) and twinning structures (- - -) diffraction. High temperature mechanical twinning is a process often reported in TiAl intermetallic

alloys [3, 6, 7] that causes a high ductility at elevate temperatures. In Fig. 8(b) a detail of 8(a) structure is reported at higher magnification, in order to put evidence of dislocation motion in γ lamellae, contained between thinner α_2 lamellae that look dark: the bowing undergone by dislocations in their attempt to move shows that it is difficult for them to penetrate into the α_2 phase and that, as a consequence, their motion tends to be confined only in γ phase. In the upper part of the same image, dislocations that belong to different γ twinning structures and do not show any acute bowing, are clearly observed, showing that γ– γ interfaces are not relevant obstacles for dislocation motion.
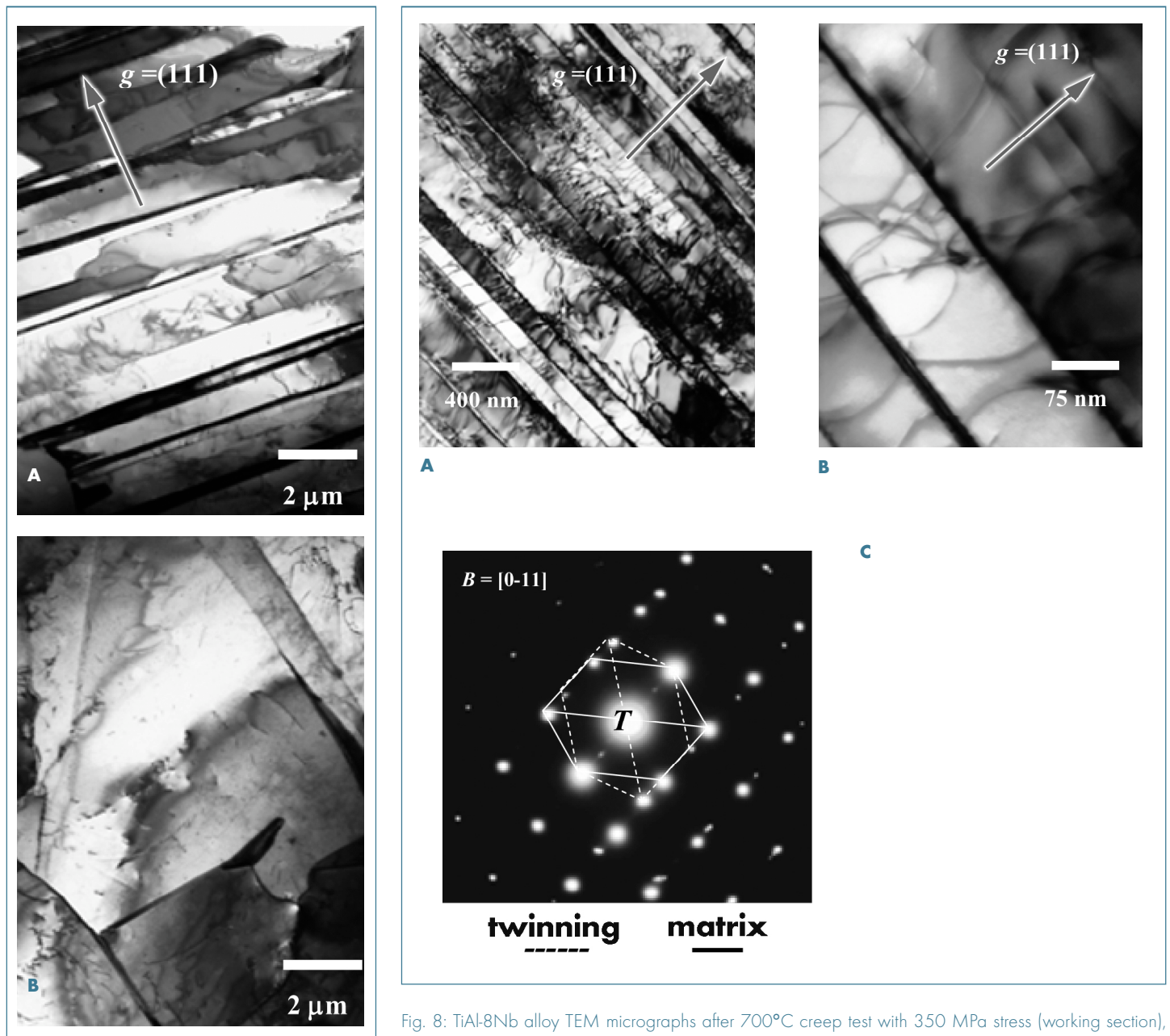

Fig. 7: TiAl-8Nb alloy TEM micrographs after 850°C creep test with zero stress (specimens heads): (a) batch E after 833 h, local axis B = [0-11]; (b) batch BN after 725 h.

Fig. 8: TiAl-8Nb alloy TEM micrographs after 700°C creep test with 350 MPa stress (working section), batch E: (a) high dislocation density mechanical twinning strain structure, local axis B = [0-11]; (b) higher magnification detail of (a), dislocation motion evidenced in γ lamellar structure; (c) correspondent diffraction image, that reveals two superimposed diffraction structures: the more intense generated from the matrix (—), the less intense from the twinning (- - -).

DISCUSSION

The significant difference between creep behaviours of the two batches is that batch E shows lower minimal strain rates $\dot{\varepsilon}_o$ and longer times to rupture than batch BN under the same creep conditions, i.e. the batch E has higher creep resistance. In TiAl alloys dislocation motion along {111} sliding planes of γ phase occurs through thermally activated mechanisms: mobile dislocations have different possible Burgers vectors [8]. The thermal stress σ^* that causes the thermally activated dislocation motion is related to external stress σ by the relationship:

$$\sigma = \sigma^* + \sigma_\mu \text{ that is } \sigma^* = \sigma - \sigma_\mu \qquad (3)$$

where σ_μ is the athermal stress, connected to obstacles that cannot be overcome thermally. The external stress σ lower than σ_μ cannot cause strain. μ is the shear modulus of the γ phase, so that σ_μ indicates that σ_μ possesses a temperature and strain rate dependence through μ only.

σ_μ refers to microstructural features that represent athermal obstacles for dislocation motion, and it has been reported [3, 9] that σ_μ is inversely proportional to square root of λ, where λ is a characteristic structural size, so that (3) becomes the Hall-Patch equation:

$$\sigma = \sigma^* + k_\lambda \cdot \lambda^{-1/2} \qquad (4)$$

k_λ is the parameter which describes the resistance of the microstructural element characterized by λ. Here, as clearly showed by Fig. 8(b), the most significant characteristic structural parameter λ, as also reported in literature on TiAl alloys [3, 9], is represented by $\alpha_2 - \alpha_2$ distance, since $\gamma - \alpha_2$ interfaces are hardly crossed by mobile dislocations that move in the soft γ phase, while $\gamma - \gamma$ interfaces are obstacles that can be easily overcome and, as a consequence, do not significantly contribute to dislocation motion resistance. The higher α_2 phase volume fraction in batch E generates a definite lamellar structure with characteristic size λ smaller than in batch BN, and consequently a smaller λ justifies why batch E shows better creep behaviour than batch BN.

As clearly showed by Fig. 8 from the creep deformed material, it can also be drawn that deformation through mechanical twinning easily happens in TiAl-8Nb intermetallic alloy. As reported in literature on TiAl alloys [6, 7] there is prevalence of mechanical twinning deformation along $\langle 11\bar{2}\rangle\{111\}$ systems over dislocation deformation, which is due to high Nb fraction that lowers γ phase Stacking Fault Energy (SFE) [10]. This hinders dislocation motion through climb, and, as a consequece, reduces dislocation contribution to the total strain. Like dislocation motion, mechanical twinning is restricted by $\gamma - \alpha_2$ interfaces [3], which further suggests that the higher α_2 phase volume fraction in batch E could cause its better creep behaviour.

Diffractometric analysis of phase volume fraction on specimens heads and working section after creep tests determined that α_2 phase has a lower volume fraction in specimens gauge than in respective heads. This phase reduction due to strain, i.e. to reduction of athermal creep mechanism obstacles through $\gamma - \alpha_2$ interfaces dissolution, could cause the accelerating regime of creep behaviour, in accordance to $\log\dot{\varepsilon}$ vs. ε plot analysis from which the damage in both batches resulted to be strain-connected rather than time-connected. This deduction could be another confirmation of the hypothesis that higher α_2 phase volume fraction increases creep resistance in TiAl alloys.

However, further microstructural research on this topic is needed in order to definitely confirm the theses exposed in this paper.

CONCLUSIONS

The alloy TiAl-8Nb, having 46Ti-46Al-8Nb nominal atomic composition, has been produced through two different solidification processes that originated two batches, i.e. E and BN, of slightly different chemical composition showing higher value of Ti/Al ratio in batch E. After solidification heat and HIPing treatments were also slightly different for the two batches. Creep behaviour study showed that batch E is more creep resistant, having lower minimum creep rates $\dot{\varepsilon}_o$ and longer times to rupture than batch BN at the same creep conditions. TEM observations showed that batch E has a finer and better defined lamellar structure than batch BN for all testing conditions, consistently with the higher α_2 phase volume fraction measured in batch E through XRD analysis.

$\gamma - \alpha_2$ interfaces are effective obstacles for dislocation motion and mechanical twinning that appear to contribute significantly to the creep deformation in TiAl-8Nb alloys. The better creep behaviour of batch E can be attributed to its better lamellar structure, caused by higher α_2 phase volume fraction because of the higher Ti/Al concentration ratio in batch E. Creep behaviour in the accelerating creep regime could be caused by α_2 phase volume fraction reduction, i.e. to the reduction of athermal creep mechanism obstacles through $\gamma - \alpha_2$ interfaces dissolution caused by strain.

Consistently, creep curves analysis in both batches showed that the accelerating regime depends on strain only rather than on time.

ACKNOWLEDGEMENTS

REFERENCES

[1] Kim Y.W. Ordered intermetallic alloys, part III: gamma-Titanium Aluminides. JOM-Journal of the Minerals, Metals & Materials Society, 1994;46(7),30.

[2] Nazmy M., Lupinc V. Gamma TiAl intermetallicsfor turbomachinery applications. Proc. 7th Liége Conference "Materials for Advanced Power Engineering 2002, vol.21 part 1, 43.

[3] Appel F., Wagner R. Microstructure and deformation of two-phase Á-Titanium Aluminides. Mat.Sci.& Eng. R 1998;22:187.

[4] Hu D., Wu X., Loretto M.H. Advances in optimisation of mechanical properties in cast TiAl alloys. Intermetallics 2005;13:914.

[5] Hu D., Huang A.J., Loretto M.H. On the massive phase transformation regime in TiAl alloys: the alloying effect on massive/lamellar competition. Intermetallics 2007;15:327.

[6] Paul J.D.H., Appel F., Wagner R. The compression behaviour of Niobium alloyed γ-Titanium Aluminides. Acta Mater. 1998;46:1075.

[7] Zhang W.J., Liu Z.C., Chen G.L., Kim Y.-W. Deformation mechanisms in a high-Nb containing γ-TiAl alloy at 900°C. Mat.Sci.& Eng. A 1999;271:416.

[8] Appel F., Oehring M., Wagner R. Novel design concepts for gamma-base Titanium Aluminides alloys. Intermetallics 2000;8:1283.

[9] Cao G., Fu L., Lin J., Zhang Y., Chen C. The relationships of microstructure and proprieties of a fully lamellar TiAl alloy. Intermetallics 2000;8:647.

[10] Song Y. , Guo Z.X., Yang R. First principles studies of TiAl-based alloys. Journal of Light Metals 2002;2:115–123.